International Journal of Heat and Fluid Flow 29 (2008) 1543–1557

Contents lists available at ScienceDirect

International Journal of Heat and Fluid Flow

journal homepage: www.elsevier.com/locate/ijhff

Growth of turbulent spots in high-speed boundary layers on a flat plate ☆

Andreas Jocksch *, Leonhard Kleiser

Institute of Fluid Dynamics, ETH Zurich, 8092 Zurich, Switzerland

ARTICLE INFO

Article history:
Received 11 November 2007
Received in revised form 18 July 2008
Accepted 3 August 2008
Available online 8 October 2008

Keywords:
Turbulent spots
Transition to turbulence
Compressible boundary layer
Supersonic flow

ABSTRACT

We investigate the development of isolated turbulent spots in supersonic flat plate boundary layers by direct numerical simulations. The spot structure is analysed and mean velocity profiles and Reynolds stresses are determined by averaging, for one flow parameter set, over an ensemble of simulations. Besides the Mach number also the Reynolds number affects the spot growth. Strong wall cooling leads to elongated turbulent spots. The asymptotic spreading of linear instabilities is investigated and its relation to the spot growth is discussed. The near-field reveals waves propagating away from the spots. Within the boundary layer they appear as distinct semi-circular patterns.

1. Introduction

The transition from disturbed laminar to fully turbulent flow can proceed along various paths. For boundary layers, the classical path is characterised by growing linear eigenmodes known as Tollmien–Schlichting waves in incompressible flow. In a later stage of transition turbulent spots appear in the otherwise ordered surrounding flow. These spots grow and subsequently merge until fully turbulent flow is developed. For an overview about transition including different ways of turbulent spot formation see Schmid and Henningson (2001).

In order to understand their spreading mechanism, the growth of isolated turbulent spots was investigated in a number of experimental studies as reviewed by Riley and Gad-el-Hak (1985). For this purpose, strong concentrated disturbances were imposed on the laminar flow which trigger localised transition. Such local turbulent spots show a number of universal properties throughout all investigations. They are indicated in the visualisation of iso-contours of the wall-normal vorticity ω_z (Fig. 1) of our simulation A1 which will be introduced later. The most noticeable property is an arrowhead-like shape where the tip of the spot is lifted away from the wall. At the tail a calmed region with streamwise-oriented streaks is established. Turbulent fluctuations are present mainly within the core region of the spot whereas in the calmed region they are suppressed.

Early direct numerical simulations (DNS) of turbulent spots in Poiseuille and boundary layer flow were performed by Henningson et al. (1987). Flow-type specific characteristic properties of the spot structure observed experimentally were confirmed, such as the overhanging front part of the boundary layer spot. The DNS of Singer (1996) (also Singer and Joslin, 1994) gave a more detailed picture of the turbulent spot in the boundary layer. The calmed region was clearly identified. It was also observed that a log-law velocity profile was beginning to establish. Further simulations were performed for turbulent spots in various shear flows, e.g., plane Couette flow (Lundbladh and Johansson, 1991) and suction boundary layers (Levin and Henningson, 2007).

The evolution of an initial disturbance in laminar flow to an incipient spot has been widely studied (for early work see Riley and Gad-el-Hak (1985)). We mention here the work of Singer and Joslin (1994) who observed that a primary hairpin vortex developed from their initial disturbance generated by localised blowing through the wall. Additional hairpin vortices form beside the primary vortex and lead to a turbulent spot. Breuer and Landahl (1990) performed a DNS of incipient spot formation in boundary layer flow. The initial disturbance was realised by a vortex pair, which was already the subject of earlier investigations, mimicking the effect of an oscillating membrane. This (or similar) vortex pair disturbances have become popular for triggering turbulent spots (Lundbladh and Johansson, 1991; Levin and Henningson, 2007) and are also used in our work.

The occurrence of waves in the near-field of turbulent spots has been a subject of vivid discussions since the experimental investigation of Wygnanski et al. (1979) who found oblique waves on the spot wingtips. The waves were suggested to participate in a local laminar-turbulent breakdown process. Waves at the tail of the

☆ This paper was originally presented at the International Symposium on Turbulence and Shear Flow Phenomena held in Munich on August 26–29, 2007, and later expanded, revised, and submitted; See Volume 29 No 3, June 2008.

* Corresponding author.
E-mail address: jocksch@ifd.mavt.ethz.ch (A. Jocksch).

0142-727X/$ - see front matter © 2008 Elsevier Inc. All rights reserved.
doi:10.1016/j.ijheatfluidflow.2008.08.008

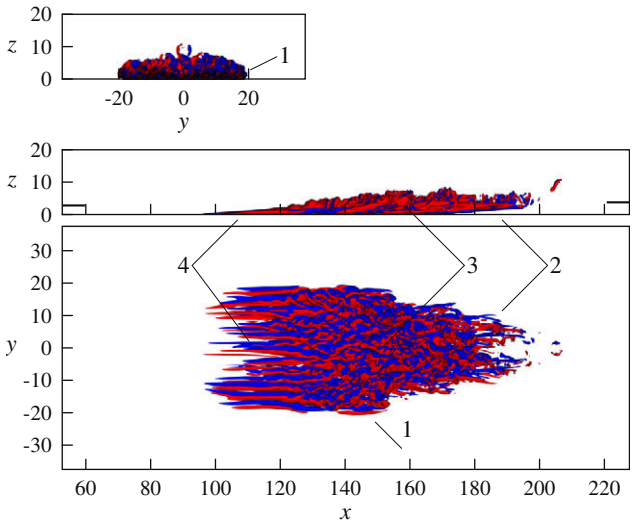

Fig. 1. Visualisations of turbulent spot with typical spot properties: (front, side and top view). (1) Wingtip with lateral overhang, (2) downstream overhang, (3) turbulent core and (4) calmed region with streaks. Thick dashes at the edges of the side view indicate the $U(z) = 0.99U_\infty$ laminar boundary layer edge. (Visualisation by iso-surfaces of $\omega_z = \pm 0.1$, case A1, single sample, $t = 228$.)

spot which appeared to passively follow the spot were observed in the experiment by Chambers and Thomas (1983). Glezer et al. (1989) argued from their measurements that waves can play different roles depending on the stability properties of the boundary layer. They can destabilise the surrounding flow or follow only passively. Singer (1996) looked for the presence of waves around his spots but found that his Reynolds number was too low and the integration time too short for the possible appearance of this phenomenon and for a comparison with the aforementioned experiments. For plane Poiseuille flow, waves on the wingtips were found in visualisations of Carlson et al. (1982). This observation was confirmed, e.g., in the simulations of boundary layer and Poiseuille flow turbulent spots of Henningson et al. (1987) which showed waves on the wingtips of the spot only in Poiseuille flow. A further numerical study of the wave phenomenon was performed by Henningson (1989). He investigated how these waves at the wingtips contribute to the growth of Poiseuille flow spots.

It is well known that for wave-induced transition scenarios the linear stability properties of the boundary layer are crucial. The spreading of turbulent spots was associated with the spreading of small disturbances in the context of front propagation (see the review of van Saarlos (2003)). These small disturbances, characterised by their dispersion relation obtained from linear stability theory, are preferably considered in the asymptotic limit of time $t \to \infty$ using the saddle-point method. How this spreading is related to the turbulent spot was discussed for Couette and Poiseuille flow. For Blasius boundary layer flow, the spreading of small disturbances was investigated in the limit $t \to \infty$ already by Gaster (1968).

The growth of small disturbances at high Mach numbers has characteristics different from the incompressible case (Mack, 1984). Some important differences are as follows. Starting around the transonic regime, for adiabatic boundary layers the least stable mode is an oblique first-mode wave (corresponding to the Tollmien–Schlichting wave in incompressible flow). Additional unstable two-dimensional higher modes appear for freestream Mach numbers $M > 2.2$. At still higher Mach numbers higher modes have a larger growth rate than the first one. Cooling of the wall stabilises the first mode but destabilises higher ones (Mack, 1984). As a consequence of multiple unstable modes at high Mach numbers, a multitude of classical wave-induced transition scenarios appear possible. Which ones are dominant at different Mach numbers was investigated by the secondary stability analysis of Ng and Erlebacher (1992), among others. One basic scenario is the so-called oblique breakdown characterised by the growth of a pair of oblique first-mode instabilities. This transition mechanism was investigated by means of DNS by Fasel et al. (1993) and Sandham et al. (1995). Alternatively, two-dimensional primary second-mode perturbations with three-dimensional secondary instabilities might dominate the process. A DNS of the subharmonic secondary-instability type was performed by Adams and Kleiser (1996) and a large-eddy simulation (LES) of this case by Stolz et al. (2007).

The topic of hypersonic transition on cones was reviewed by Schneider (2004) who also reproduced a visualisation of a turbulent spot including noise radiation from the turbulent region. Fischer (1972) discussed the influence of the Mach number on the spreading of turbulent disturbances based on a comprehensive collection of experimental results, not only from turbulent spots but also from other spreading disturbances like those behind roughness trips. Despite a large scatter of the data a clear decrease of the lateral spreading with increasing Mach number was found. Measurements on naturally occurring turbulent spots in subsonic and supersonic boundary layers along flat plates were performed by Clark et al. (1994), de Lange et al. (1998) and Mee (2002). They detected turbulent spots and their growth from heat transfer measurements at the wall. It appeared that a mechanism of spot generation and growth took place which was similar to the incompressible case. The lateral spreading was reduced for higher Mach numbers. Recently, DNS of spot growth in supersonic boundary layers at $M = 2$, 4 and 6 were performed by Krishnan and Sandham (2006a,b). Their turbulent spots showed the typical structures known from the incompressible case. The reduced lateral spot growth with increasing Mach number was confirmed. At $M = 6$ additional spanwise structures were observed. The aspects of spot growth mechanisms, spot merging (Krishnan and Sandham, 2006b) and the interference with a shock-induced separation bubble (Krishnan and Sandham, 2007) were also investigated.

In the present contribution, we study the growth of isolated turbulent spots in laminar zero pressure gradient boundary layers on a flat plate at $M = 1.1$ and 5 by DNS. After briefly describing the numerical approach we present results for transonic boundary layer spots. The spot structure is discussed and for one parameter set turbulence statistics are evaluated based on ensemble-averaging 40 separate simulations with slightly varying initial conditions. Further topics of consideration are the Mach and Reynolds number influence and the effect of wall cooling. For $M = 5$ the spreading of turbulent spots is put in relation to the growth of linear disturbances in the limit $t \to \infty$. The near-field of the spots is investigated with respect to the occurrence of waves. Also for $M = 5$ one dominant wave pattern is analysed with respect to basic types of eigenmodes of the inviscid linear stability theory.

2. Simulation method

We consider supersonic isothermal-wall boundary layers on a flat plate. The Navier–Stokes equations for a perfect gas are numerically solved in a rectangular box. The ratio of specific heats amounts to $\gamma = 1.4$ and a constant Prandtl number of $Pr = 0.72$ is chosen. Sutherland's law determines the viscosity with the constant $Su = Su^*/T^*_\infty = 110\ \mathrm{K}/293\ \mathrm{K}$ where T^*_∞ is the freestream temperature (*denotes dimensional values). At the outer edge of the computational domain non-reflecting boundary conditions are applied. Dirichlet boundary conditions with sponge zones are used at the inflow and outflow boundaries. In the spanwise direction periodicity is applied.

To specify the initial and boundary conditions a boundary layer similarity solution according to the Howarth–Dorodnitsyn transformation (Stewartson, 1964) is used. At moderate Reynolds numbers, appreciable differences exist between the boundary layer approximation and the Navier–Stokes solution which are on the order of the small physical disturbances present in our simulations. Therefore, in our simulations a forcing term is applied to the Navier–Stokes equations which maintains the laminar boundary layer solution when no disturbances are present. Our computational domain employs an optional frame of reference moving downstream at constant speed. At the starting time it is at rest with respect to the wall. When the disturbance has travelled to the middle of the box the reference frame velocity is set to the approximate spot centre velocity. This allows to shorten considerably the streamwise box length.

A compact finite-difference scheme of third-order at the boundary points, fourth-order at the points adjacent to the boundary and sixth-order in the interior for first- and second-derivative operators (Lele, 1992) is used for spatial discretisation and a grid stretching is applied in the wall-normal direction. Either a low-storage third-order Runge–Kutta method (Williamson, 1980) or the classical fourth-order Runge–Kutta method are employed for time marching. The convective terms are expressed in skew-symmetric form following Honein and Moin (2004) to enhance numerical stability. The diffusive terms are evaluated using second-derivative operators to damp gridpoint-to-gridpoint oscillations (see e.g. Sandham et al. (2002)).

As initial disturbance a vortex pair is superimposed on the laminar boundary layer solution. We adopt the disturbance streamfunction definition used by Breuer and Landahl (1990) for triggering localised disturbances in incompressible flat plate boundary layer flow,

$$\Psi = \epsilon \cdot (x/l_x)(y/l_y)(z/l_z)^3\, \mathrm{e}^{-(x/l_x)^2-(y/l_y)^2-(z/l_z)^2} \tag{1a}$$

$$(\rho u)' = 0, \quad (\rho v)' = \Psi_y, \quad (\rho w)' = -\Psi_z \tag{1b}$$

where $[(\rho u)',(\rho v)',(\rho w)']$ is the disturbance of the momentum and ρ the density. Here (x,y,z) and (u,v,w) denote the coordinates (fixed to the wall) and velocities, respectively, in the streamwise, spanwise and wall-normal directions. The dimensions of the vortex pair are $l_x = 10/3$, $l_y = 4$, $l_z = 4/5$ and the strength is $\epsilon = 1$ for all simulations. Lengths are normalised throughout this paper with the displacement thickness δ_1^* at the triggering position of the spot. Velocity, density, temperature, and kinematic viscosity are normalised with the freestream values U_∞^*, ρ_∞^*, T_∞^*, ν_∞^* respectively, the pressure p with $\rho_\infty^* {U_\infty^*}^2$ and time t with δ_1^*/U_∞^*. Accordingly, the Reynolds number is defined as $Re \equiv Re_{\delta_{1\infty}} = U_\infty^* \delta_1^*/\nu_\infty^*$. Other Reynolds numbers are $R = (U_\infty^* x_{lp}^*/\nu_\infty^*)^{1/2}$, $Re_\theta = U_\infty^* \delta_2^*/\nu_\infty^*$ and $Re_{\delta_2} = \rho_\infty^* U_\infty^* \delta_2^*/(\rho_w^* \nu_w^*)$, where δ_2^*, x_{lp}^*, ρ_w^* and ν_w^* are the momentum thickness, the distance from the leading edge of the plate, the density and viscosity at the wall, respectively.

3. Spot development

We begin with considering a transonic boundary layer transition at $M = 1.1$ and $Re = Re_{\delta_{1\infty}} = 800$, denoted as case A1. The wall temperature of our simulations is that of the adiabatic laminar boundary layer solution unless mentioned otherwise. The parameters M, Reynolds numbers and wall-to-freestream temperature T_w/T_∞ are given in Table 1. Furthermore, the extent of the computational domain L_x, L_y, L_z in the streamwise, spanwise and wall-normal directions and the corresponding number of grid points N_x, N_y, N_z are included. (The third-order temporal discretisation was used for this case and the fourth-order one for all following cases.)

Because of the lack of any temporal or spatial homogeneity, statistical properties are determined by averaging over an ensemble of 40 different realisations of the spot development. In experimental work ensemble-averaging has been applied similarly, e.g., for the investigation of substructures in the spot (Sankaran et al., 1988) and other detailed statistical analysis (Schröder and Kompenhans, 2004). In order to provide different realisations of the spots, we trigger them with additional small random disturbances (u_n, v_n, w_n) superimposed at $t = 0$ on the vortex pair disturbing the laminar boundary layer solution. The random homogeneous isotropic noise has an energy spectrum with a Fourier amplitude distribution according to

$$|\hat{u}_n| = |\hat{v}_n| = |\hat{w}_n| = \frac{1}{4000}\left(\frac{|k|}{k_p}\right)^8 \exp\left[-2\left(\frac{|k|}{k_p}\right)^2\right] \tag{2}$$

(k = wavenumber, $k_p = 4.2$). The phases of the complex Fourier modes were chosen randomly (distributed uniformly over $[0,2\pi)$) where the set of all random phases is independent for each simulation. This homogeneous noise is modulated with the shape of the vortex pair disturbance, resulting in

$$[(\rho u)'(u_n+1), (\rho v)'(v_n+1), (\rho w)'(w_n+1)] \tag{3}$$

as the actual disturbance imposed on the initial flow field. This way the noise only affects the main disturbance (but not the surrounding laminar flow) and is made inhomogeneous, realising especially the zero velocity at the wall. The slight spanwise asymmetry of the spots generated by this method is exploited to double the statistical sample size by averaging over spanwise mirror positions across the plane $y = 0$.

Breuer and Landahl (1990) investigated how strong initial disturbances develop as opposed to weak ones. We chose an initial disturbance strong enough to cause a fast development into a turbulent spot in the sense that the breakdown to turbulence occurs before disturbances have extended significantly over the whole computational domain. If the initial disturbance is too weak this may lead to very long elongated structures before the flow becomes turbulent. Overall, the development of the initial disturbance in the compressible boundary layers investigated is similar to the incompressible case of Breuer and Landahl (1990).

Fig. 2 shows the development of early structures by iso-contours of the second invariant $\lambda_2 = -10^{-2}$ of the velocity gradient tensor (vortex detection criterion) of a single realisation for case A1. Comparing the visualisations of λ_2 at different times gives insight into the disturbance development. Singer and Joslin (1994) and Krishnan and Sandham (2006a) found a primary hairpin vortex arising immediately after triggering by localised blowing through the wall. Afterwards further neighbouring hairpin vortices developed. We do not observe this sole hairpin vortex and subsequent

Table 1
Flow and simulation parameters for the five cases investigated ($Re = Re_{\delta_{1\infty}}$)

	M	R	$Re_{\delta_{1\infty}}$	Re_θ	Re_{δ_2}	T_w/T_∞	L_x	$L_y/2$	L_z	N_x	N_y	N_z
A1	1.1	362.0	800	237	205	1.20	175	37.5	37.5	767	384	192
A2	1.1	678.8	1500	444	385	1.20	175	37.5	37.5	1580	385	385
B1	5.0	305.6	3000	163	56	5.19	250	54	37.5	1116	294	294
B2	5.0	509.4	5000	271	93	5.19	210	51	37.5	1900	525	595
C	5.0	699.6	3000	429	429	1	210	37.5	37.5	988	207	299

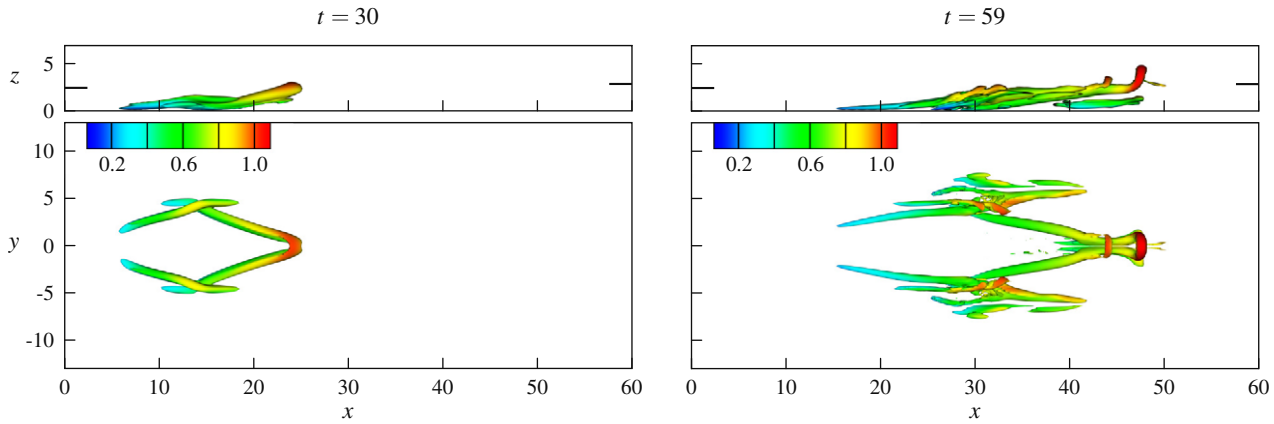

Fig. 2. Visualisation of incipient spot development by iso-surfaces of $\lambda_2 = -10^{-2}$, coloured with velocity magnitude (dark: low values, light: high values in all figures of the printed version, full colour in the online version). $M = 1.1$, $Re = 800$ (case A1), single sample, side and top view.

development, which can be attributed to the different triggering procedure. Rather, the first hairpin is accompanied by further structures at its tail forming a diamond. These interact and form more complex topologies at the side vertices while at the tip of the hairpin also secondary hairpins appear.

Some time after the development of these early structures a localised turbulent region is established. Fig. 3 shows iso-contours of $\lambda_2 = -10^{-5}$ for this development. (The same iso-value is chosen for all visualisations except Fig. 2.) At the later stage $t \approx 170$, a vortex system at the tip appears like in Singer and Joslin (1994). The developed turbulent spot at $t = 228$ shows typical universal properties known from previous investigations. The plan-view shape is arrowhead-like and there is a downstream overhang region (cf. Fig. 1). At the tail region elongated streamwise structures, so-called streaks, dominate which are pronounced in the ω_z visualisation. The turbulent spot grows out of the laminar boundary layer, which appears plausible if the turbulent part behaves similarly to a turbulent boundary layer which is known to grow faster than a laminar one. The semi-circular structures appearing in the near-field of the turbulent spot at $t = 59$ (Fig. 3) and again in the developed stage ($t = 228$) will be discussed later. (Spanwise structures seen at the inflow and outflow developing at the final stage $t = 228$ are artefacts due to the limited domain size.)

It is of obvious interest to consider statistical quantities in the spot region and to compare these with known turbulence proper-

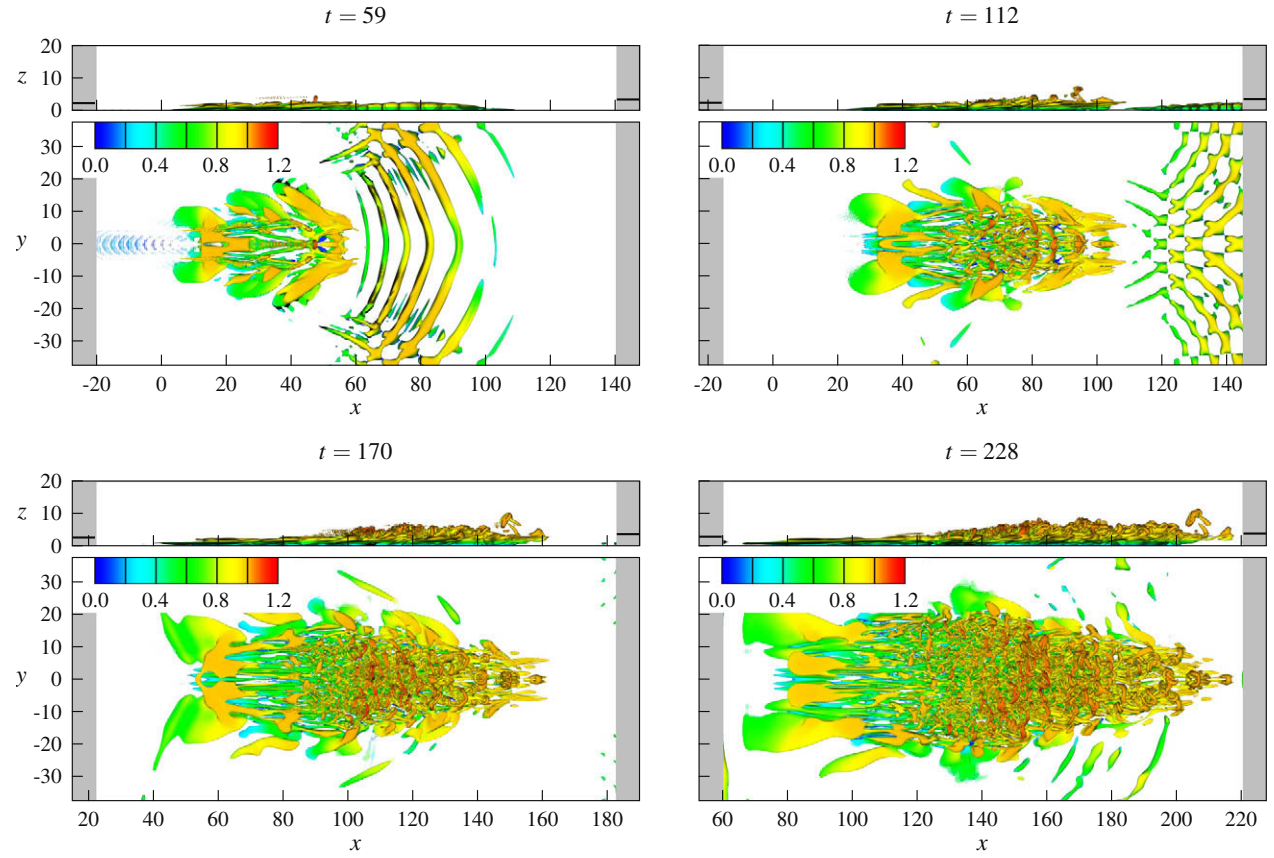

Fig. 3. Visualisation of spot development by iso-surfaces of $\lambda_2 = -10^{-5}$, coloured with velocity magnitude. Case A1, single sample, side and top view. Grey bars in this and later figures mark the sponge region.

ties, using the ensemble-averaging mentioned earlier. The average of a quantity q is denoted as $\bar{q}$, its Favre-average as $\tilde{q} = \overline{\rho q}/\bar{\rho}$. Fig. 4 shows profiles of the Favre-averaged velocity components $(\tilde{u}, \tilde{v}, \tilde{w})$ in planes normal to the spanwise direction at $y = 0$, $y = 7.5$ and $y = 15$, respectively. Profiles of the Favre-averaged temperature $\tilde{T}$ and the inverse averaged density $1/\bar{\rho}$ are also shown, which largely coincide due to the almost constant pressure within the domain. Deviations from the laminar profiles within the spot region are clearly visible. At the tail of the spot smooth velocity profiles with gradients at the wall steeper than the laminar ones are present indicating the calmed region. Velocity and temperature deviations from laminar values in selected planes are visualised in Fig. 5. It is apparent that the whole spot region is streaky.

In order to visualise the crossflow, sectional streamlines and velocity vectors $(\tilde{v}, \tilde{w})$ of the spanwise and wall-normal components in planes $x = \text{const.}$ are shown in Fig. 6. The wall-normal velocity above the core of the turbulent region is significantly larger than for the laminar boundary layer (see Fig. 6 for $x = 150$). The freestream is displaced outward by the central part of the spot. The turbulent spot is laterally embedded by sectional streamlines. In the upstream and downstream parts of the spot ($x = 120$, $x = 180$, respectively) the wall-normal velocity component is partially di-

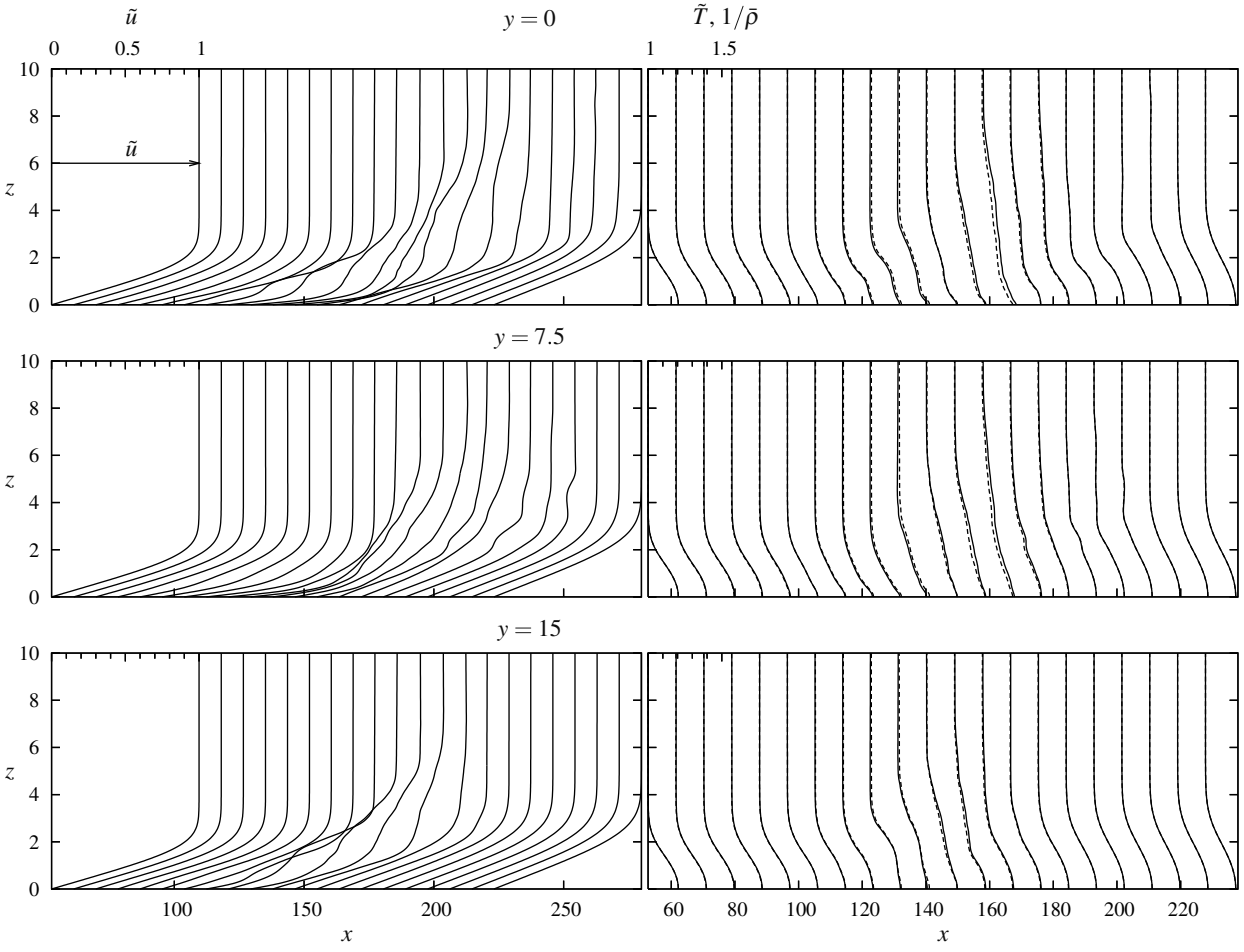

Fig. 4. Profiles of Favre-averaged streamwise velocity $\tilde{u}$ (left), temperature $\tilde{T}$ —— and inverse average density $1/\bar{\rho}$ ---- (right) in three planes $y = \text{const.}$ Case A1, $t = 228$.

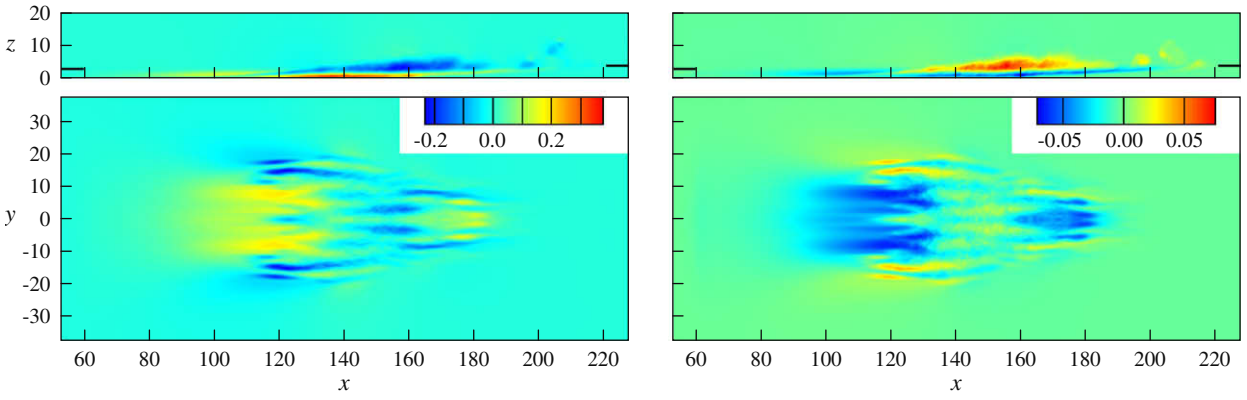

Fig. 5. Deviation of streamwise velocity $\tilde{u} - U$ (left) and temperature $\tilde{T} - T$ (right) from laminar values, side view of mid-plane and top view of $z = 1.51$ plane. Case A1, $t = 228$.

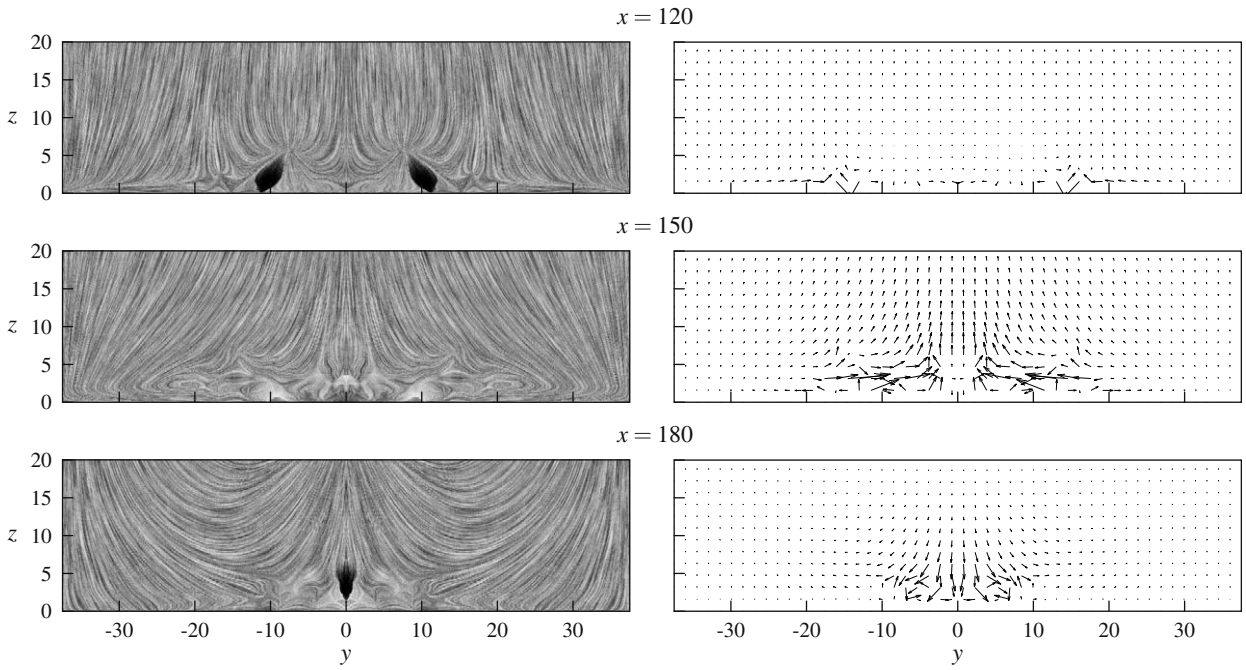

Fig. 6. Sectional streamlines (left) and projected velocity vectors $(\tilde{v}, \tilde{w})$ (right) of the averaged velocity field in $y - z$ planes. The maximum vector length refers to a velocity of $|(\tilde{v}, \tilde{w})|_{\max} = 0.078$. Case A1, $t = 228$.

rected toward the wall. These observations are consistent with the principal spot structure derived from investigations of turbulent spots in incompressible boundary layer flow like the early ones referenced in Riley and Gad-el-Hak (1985).

Statistics of disturbances are considered next. The streamwise Reynolds normal stress $\bar{\rho}\widetilde{u''u''}$ and the Reynolds shear stress $-\bar{\rho}\widetilde{u''w''}$ are depicted as profiles in Fig. 7 and by section planes in Fig. 8. The shape of the two Reynolds stress distributions looks quite similar. Strong fluctuations are visible in the core of the spot and at the lateral tails, whereas in the region of the tip vortex system and the tail the fluctuations are rather small.

We note that the distribution of the Reynolds stresses within the turbulent spot (Figs. 7 and 8) compared with the structures of a single realisation (Fig. 3) shows that in the region of dominant turbulent fluctuations hairpin structures are present similarly as in fully developed turbulent boundary layers. Hairpin structures are also present at the tip of the spot where fluctuations are moderate. This we interpret as follows. While in the interior of the spot the flow is close to being fully turbulent, at the tip it is rather early transitional. The hairpin structures occur more sparsely and turbulent motions are only present in a limited layer which does not extend down to the wall (lifted tip).

The local distribution of the skin-friction coefficient c_f is shown in Fig. 9. It becomes visible that the c_f distribution is streaky not only in the tail region but in the whole spot. The picture is similar to the ones given by deviations of streamwise velocity and temperature (Fig. 5) in a near-wall plane. Other ensemble-averaged quantities are also streaky inside the turbulent core as, e.g., the wall-normal vorticity (not shown). For the latter quantity streakiness was shown earlier for ensemble-averaged spots in incompressible boundary layer flow by Schröder and Kompenhans (2004). The dominant streaks outside the calmed region are a result of the averaging procedure, while a single realisation of the turbulent spot shows a more chaotic pattern. Despite the averaging procedure the streamwise and spanwise distributions of c_f remain spiky.

The core region of the spot may be related to fully turbulent boundary layers. In order to provide a comparison, representative

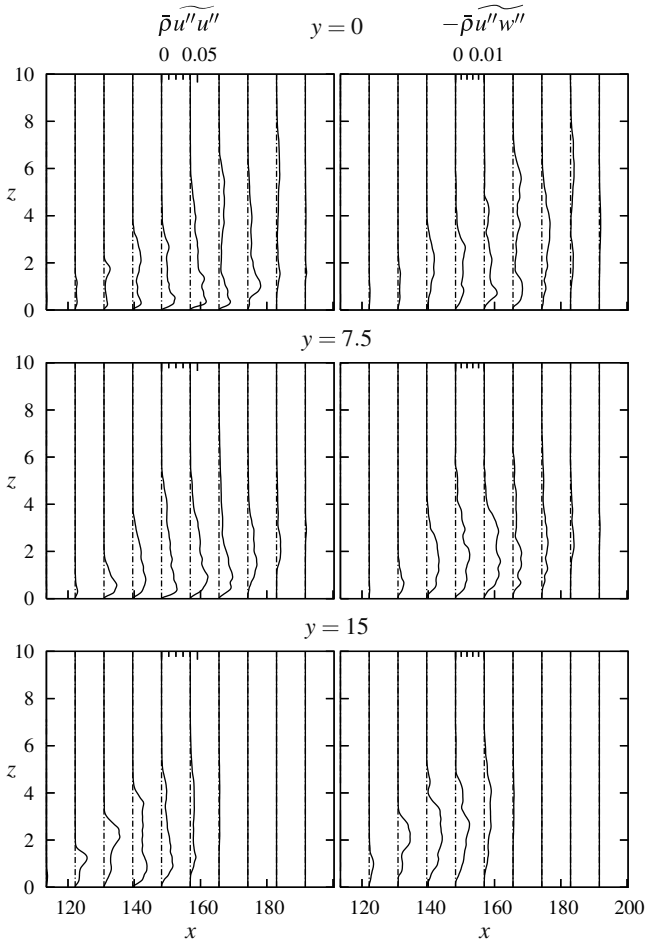

Fig. 7. Profiles of Reynolds normal stress $\bar{\rho}\widetilde{u''u''}$ (left) and Reynolds shear stress $-\bar{\rho}\widetilde{u''w''}$ (right) in three planes y = const. Case A1, $t = 228$.

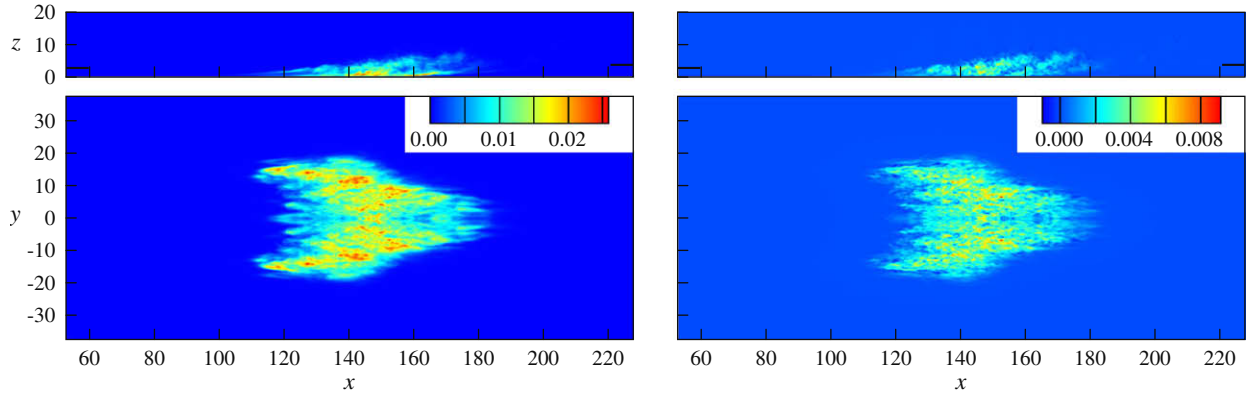

Fig. 8. Reynolds normal stress $\bar{\rho}\widetilde{u''u''}$ (left) and Reynolds shear stress $-\bar{\rho}\widetilde{u''w''}$ (right), side view of mid-plane and top view of $z = 1.51$ plane. Case A1, $t = 228$.

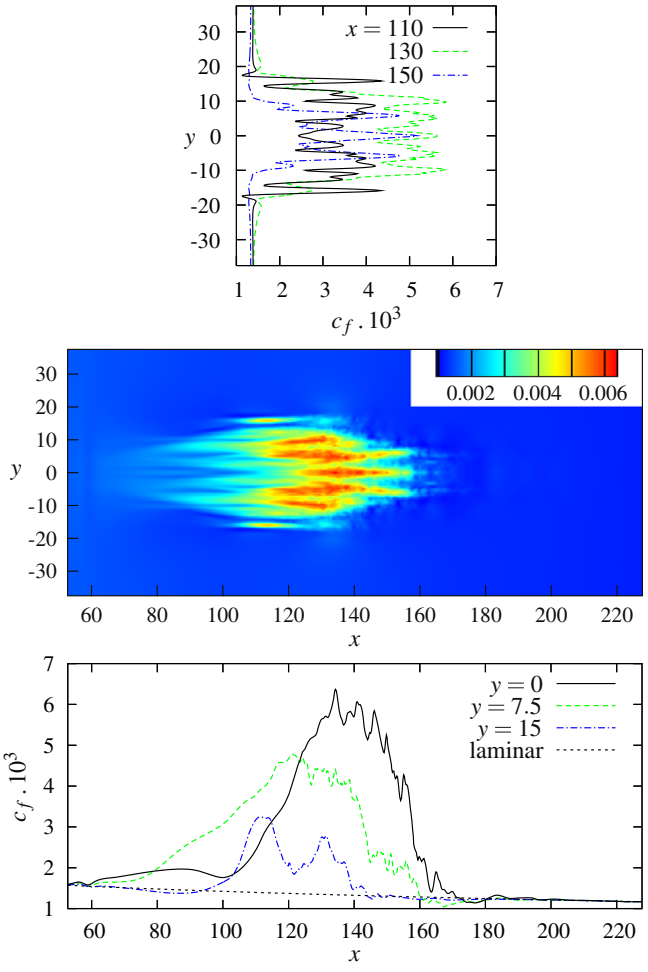

Fig. 9. Local skin-friction coefficient c_f of ensemble-averaged spot. Case A1, $t = 228$.

profiles are determined by additional local averaging over a rectangular domain $[x_{a1},x_{a2}] \times [-y_a,y_a]$ within the spot core (see Table 2). From these profiles, the friction velocity $u_\tau = \sqrt{\tau_w/\rho_w}$ and the wall reference length $v_w/(u_\tau Re)$ are determined where $v_w = v_w^*/v_\infty^*$ is the (non-dimensional) viscosity, τ_w the shear stress and ρ_w the density at the wall, respectively (Table 2). The quantities $z^+ = u_\tau z Re/v_w$ and $u^+ = u/u_\tau$ measured in wall units are introduced and the velocity profiles are shown in Fig. 10 incorporating van Driest's transformation $u_{VD}^+ = \int_0^{u^+} \sqrt{\rho/\rho_w}\,du^+$. As found by Singer (1996) and Krishnan

Table 2
Reynolds numbers and grid spacings in wall units of the turbulent spot core

	x_{a1}	x_{a2}	y_a	u_τ	$u_\tau Re/v_w$	$Re_{\delta_1,\infty,t}$	$Re_{\delta_2,t}$	Δx^+	Δy^+	Δz_w^+
A1	116.5	141.6	7.81	0.0531	30.98	890	420	7.08	6.05	0.760
A2	84.9	114.9	6.84	0.0531	58.08	1500	780	6.44	5.67	0.707
B1	241.8	275.4	9.21	0.0634	12.93	7680	360	2.90	2.38	0.320
B2	156.9	176.8	6.81	0.0567	20.74	7870	580	2.29	2.02	0.252
C	181.0	204.4	2.73	0.0308	93.07	4850	1140	19.8	16.94	2.26

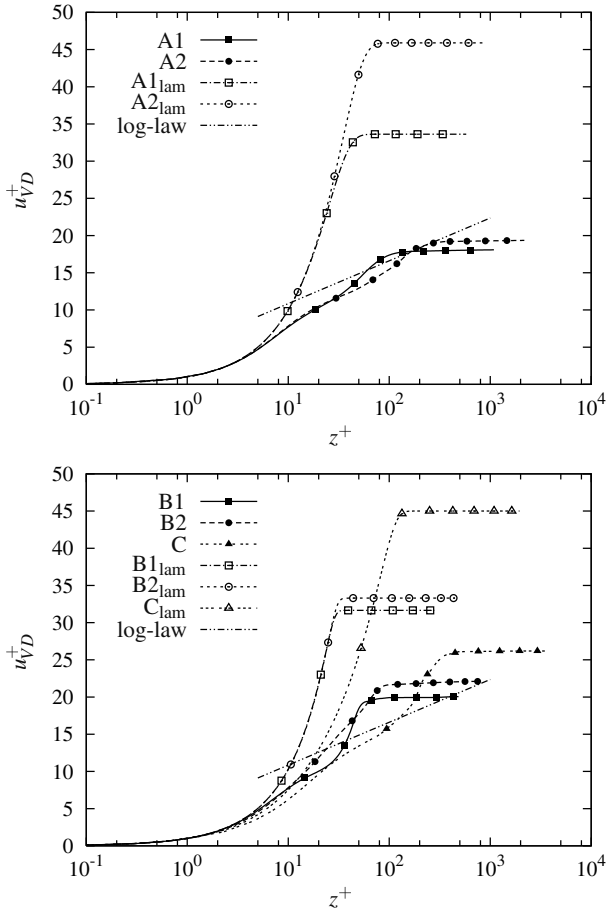

Fig. 10. Van-Driest-transformed mean velocity profiles of the turbulent spot core for the various cases of Table 2 and logarithmic law of the wall $u^+ = 2.5 \cdot \ln y^+ + 5.1$. $(\,)_{\text{lam}}$ represents the transformed undisturbed laminar boundary layer.

and Sandham (2006b), the region characterised by the log-law is only partially developed at this stage of transition. This is not only attributed to the non-homogeneous flow field but also to the generally low Reynolds number. The Reynolds numbers based on the local displacement thickness, $Re_{\delta_{1_{\infty,t}}}$, and local momentum thickness, $Re_{\delta_{2,t}}$, of the turbulent core at $t = 228$ are listed in Table 2.

The distance between the spanwise streaks at the tail (Fig. 1) amounts to approximately 80 wall units, as found for turbulent spots in incompressible boundary layers (Riley and Gad-el-Hak, 1985). This is only slightly below the commonly quoted spacing of the streaks in the viscous sublayer of fully developed wall turbulence. The streaks in the front region visible in the c_f values have a larger spacing. The grid resolutions in our local wall units are also given in Table 2. Δx^+ and Δy^+ denote the equidistant spacings in x and y direction, Δz_w^+ the wall-normal spacing of the point closest to the wall. These resolutions are similar to those of Krishnan and Sandham (2006a) for turbulent spots and of Pirozzoli et al. (2004, and references therein) for fully turbulent boundary layers.

4. Higher Mach and Reynolds numbers

We now turn to supersonic boundary layer flows at $M = 5$. Also, Reynolds number effects are considered at both Mach numbers: cases A1 and B1 are complemented by the corresponding cases A2 and B2 at higher Reynolds numbers. Furthermore, we investigate the effect of wall cooling at $M = 5$ (case C). Table 1 summarises the respective flow and simulation parameters. Apart from case A1, we apply a spanwise-symmetry condition at the mid-plane $y = L_y/2$ in all cases and simulate only a single realisation (without superimposed noise). On the one hand, this suppresses any potentially asymmetric flow structures. On the other hand, the saved computational effort can be invested into a larger box size and/or higher resolution to investigate other spot features of particular interest, e.g., the near-field. Experiments and simulations with broken symmetry (such as case A1 in the present contribution or Levin and Henningson (2007)) indicate that turbulent spots are likely to develop naturally in a quite symmetric manner.

The transonic flow case A2 with increased Reynolds number at the triggering position (Fig. 11) shows a similar principal spot structure as the lower Reynolds number case A1 (Fig. 3). In particular the vortices at the tip and the structures at the wingtips and the tail look similar. The turbulent structures in the core become finer for the higher Reynolds number due to reduced viscous damping and the streaks at the tail become less dominant. The higher Reynolds number at the triggering position leads to an enhanced growth of the spot and results in a larger extent of the spot at an earlier time compared to the lower Reynolds number case (see also Section 5). A similar result is found for spots in the high-supersonic regime which will be discussed below. It is supposed that the additional noise in the initial disturbance of case A1 does not impair the comparability between the different cases.

Straightforward comparisons of results at different Mach numbers are difficult with respect to Reynolds number effects. The transitional process is supposed to be dominated by different physical phenomena which are characterised by their specific Reynolds number. The critical Reynolds number for linear instability is attributed to play some role in the transitional process (For critical Reynolds numbers at different Mach numbers see Mack (1969)). The Reynolds numbers Re_{δ_2} and Re_θ are significant for fully turbulent boundary layers and also assumed to be relevant here. Due to the properties of the laminar boundary layer these different Reynolds numbers cannot be kept constant for a changing Mach number. Thus, for the present investigation, the Reynolds number was chosen heuristically to provide a similar development of the disturbance. It always refers to a triggering position within the linearly unstable domain. Table 1 includes values of the various Reynolds numbers. A similar problem of comparability arises with providing the same strength of the triggering (Eq. (1b)). The size of the initial vortex pair disturbance could be related as well to a reference scale other than the displacement thickness employed.

Overall the turbulent spots at $M = 5$ (Figs. 12 and 13) show the typical features already observed in the transonic boundary layer.

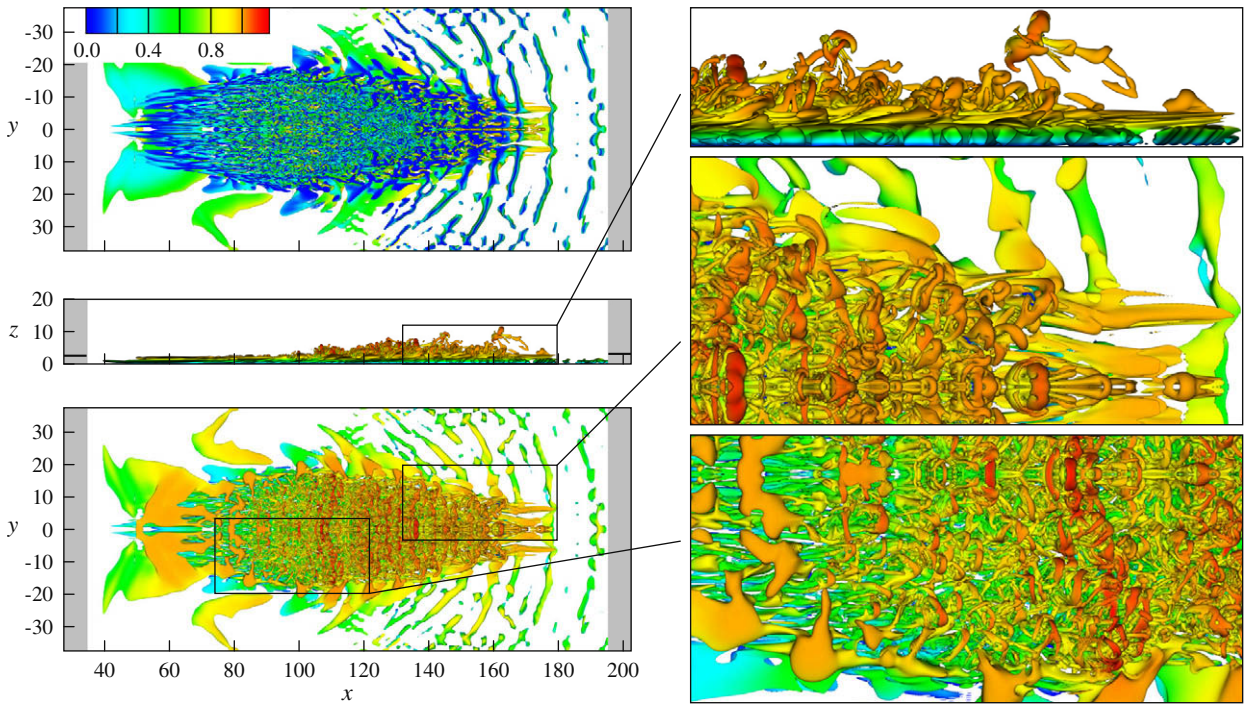

Fig. 11. Iso-surfaces of $\lambda_2 = -10^{-5}$ coloured with velocity magnitude, $M = 1.1$, $Re = 1500$ (case A2), $t = 185$. Bottom-view (top), side view (middle) and top view (bottom).

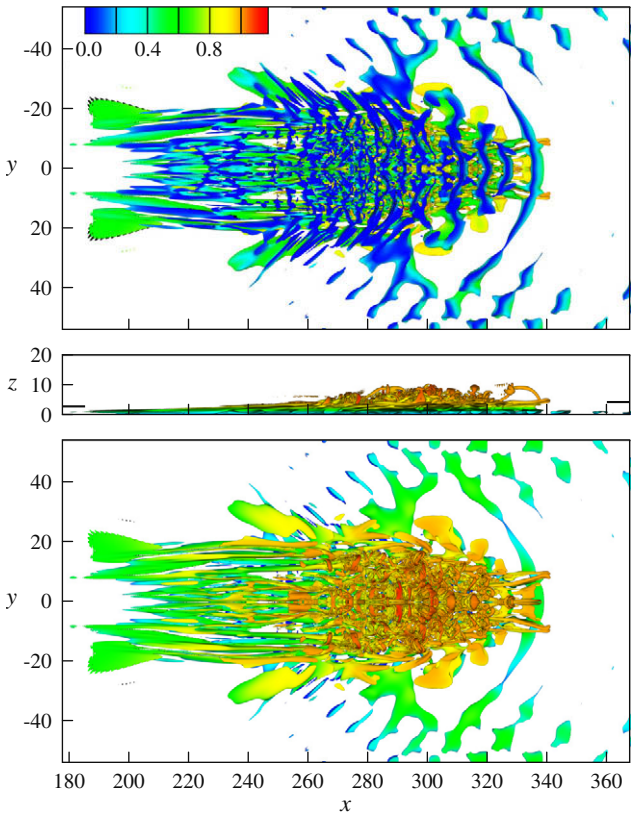

Fig. 12. Iso-surfaces of $\lambda_2 = -10^{-5}$ coloured with velocity magnitude, $M = 5$, $Re = 3000$ (case B1), $t = 338$. Arrangement as in Fig. 11 (left).

Unlike in the transonic case, at $M = 5$ below the spot dominant spanwise structures close to the wall are present during the whole spot formation process. Spanwise structures were also observed by Krishnan and Sandham (2006a) in their $M = 6$ case. For the final stage of case B1, $t = 228$, starting from the tip of the turbulent spot these spanwise-directed structures are present and decrease in magnitude toward the centre of the spot (Fig. 12, bottom and side view). From the centre to the tail spanwise-directed structures are not dominant anymore. Our simulation at higher Reynolds number, case B2, shows a very similar phenomenon (see bottom view of Fig. 13). The spanwise-directed structures are larger and more ordered compared to the typical hairpin vortices (visible in the top views) which are located farther away from the wall above them. Their streamwise propagation velocity is slightly smaller than the freestream velocity. The semi-circular structures in the near-field, which will be discussed in Section 7, propagate faster than the spanwise structures in the spot region. We consider the occurrence of spanwise structures as a purely transitional phenomenon. The region from the tip to the centre of the spot where they appear is the region where the local transition process takes place. As far as we are aware published investigations of fully developed compressible turbulent boundary layers and of wave-induced transition do not indicate any dominance of large-scale spanwise structures.

In order to investigate the effect of the wall temperature, an additional simulation (case C) was performed with a cooled wall in which the wall temperature was set equal to the freestream temperature. The corresponding iso-surfaces of λ_2 (Fig. 14) show a quite different spot shape compared to the adiabatic wall case (Figs. 12 and 13). The spot is highly elongated with a dominant tail. The dominant spanwise structures in the front region of the spots found for cases B1 and B2 are hardly detectable here. Rather, spanwise structures interact with the streamwise structures in the tail region. In the near-field again semi-circular structures are present.

As for case A1, profiles averaged over a small rectangular subdomain within the spot core have been obtained. Naturally, the choice of the subdomain significantly influences the resulting average values, which therefore are valid only locally. While for case A1 averaging was based in addition on 40 samples, in the other cases only one realisation of the turbulent spot was available. Note that Krishnan and Sandham (2006b) analysed a further developed turbulent spot at $M = 2$. Thus their average values from the core region should be statistically more significant and less sensitive to the choice of the averaging domain. The logarithmic profile is also only partially developed in all these other cases (Fig. 10). Note that the standard log-law is well established for adiabatic boundary layers, while for cooled walls a modified additive constant applies (Maeder, 2000, and references therein). As already mentioned for case A1, the grid resolutions in wall units for case A2 are similar to those of turbulent spot and fully developed turbulent boundary layer simulations in the literature. The grid spacings of cases B1 and B2 are rather small compared to those commonly used for fully turbulent flow (Pirozzoli et al., 2004). For case C the grid spacings are approximately twice those for fully developed turbulent boundary layers with strong wall cooling by Maeder (2000).

5. Spot growth and Reynolds number dependence

Early experiments (see Riley and Gad-el-Hak (1985)) report a self-similarity of turbulent spots based on a linear growth of the spot size which is quantified by its constant spreading half-angle. As already mentioned, Fischer (1972) reported a reduction of the growth rate with increasing Mach number. Fig. 15 shows the location of the front, tail and lateral spot edges (defined by $|\omega_z| = 0.1$) as a function of time. Lateral spreading half-angles, shown in Table 3, are estimated from our spot simulations and are defined as $\arctan(\Delta y_{la}/\Delta x_c)$ where the centre of the spot x_c is the average between the leading edge and trailing edge position and y_{la} is the lateral edge position. The growth is measured by linear regression between $t = 150$ and the final stage of the simulations. The trend of decreasing spreading half-angles with increasing Mach number is confirmed. However, the Reynolds number at the triggering position also has a strong influence on the observed spreading half-angle, which increases with Reynolds number. Also the nonlinear spot growth in the late stages of development indicates different spreading characteristics with the downstream-increasing Reynolds number. The Reynolds number effect is known from parallel (fixed Reynolds number) flows such as plane Couette flow (Lundbladh and Johansson, 1991). For boundary layers, where the Reynolds number is continuously increasing in downstream direction, Singer (1996) found an increase of the spreading half-angle with rising Reynolds number. His evaluation of earlier experiments indicated some Reynolds number dependence of the spot development. However, Singer (1996) noted that his Reynolds number based on the distance from the triggering position to the location of the finally developed spot of his simulation was too low for a direct comparison with these experimental references. In our study for all cases the time span of spot development is also rather short.

At the latest stages of spot development of cases A1 and A2 the computational domain is largely occupied by the spot and therefore the growth should be influenced by the boundaries, respectively the spanwise-periodic neighbours. While for case C the length of the box is also exhausted, for cases B1 and B2 more space is left.

Compared to the present ones, very long developed turbulent spots have the distinctive property of a large wall-normal extent

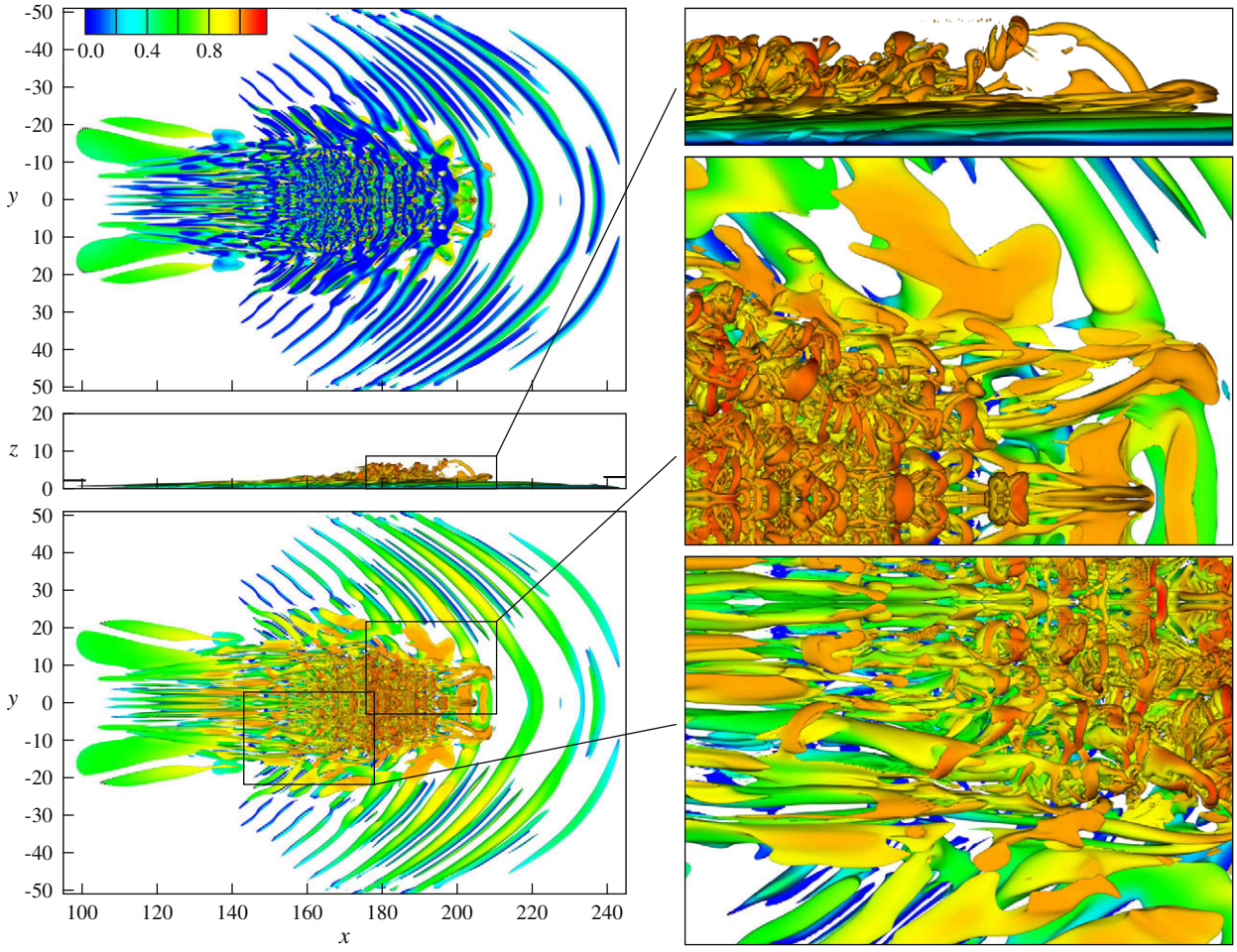

Fig. 13. Iso-surfaces of $\lambda_2 = -10^{-5}$ coloured with velocity magnitude, $M = 5$, $Re = 5000$ (case B2), $t = 207$. Arrangement as in Fig. 11.

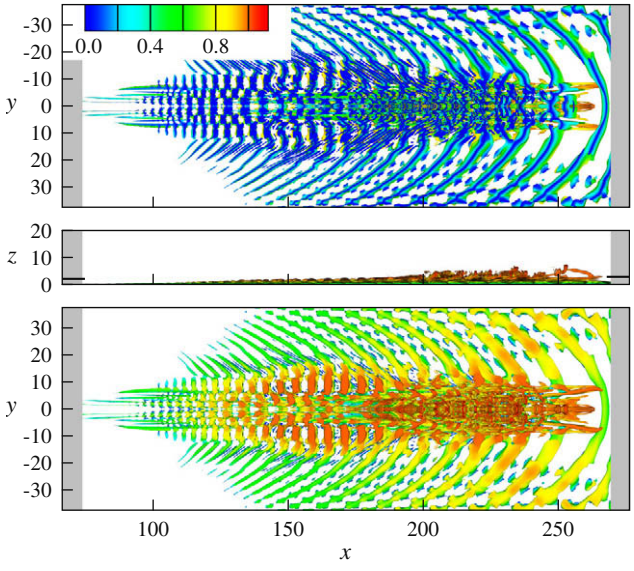

Fig. 14. Iso-surfaces of $\lambda_2 = -10^{-5}$ coloured with velocity magnitude, $M = 5$, $Re = 3000$, cooled wall $T_w = T_\infty$ (case C), $t = 264$. Arrangement as in Fig. 11 (left).

compared to the thickness of the surrounding laminar boundary layer. It is expected that at a stage of spot development much later than in our cases the Reynolds number effect diminishes and the spreading is primarily affected by the Mach number.

6. Spreading of disturbances

In the following, we attempt to give some explanation for the different nature of the turbulent spots at $M = 5$ for the adiabatic and cooled wall cases by means of linear stability theory. Compressible boundary layers show several distinct linear stability properties which were comprehensively investigated and reviewed by Mack (1984). Some of these properties are: If an inflexion point $(U'/T')(z_c) = 0$ exists such that $U(z_c) > 1 - 1/M$ inviscidly unstable eigenmodes are present (generalised inflexion point criterion), where $z = z_c$ denotes the critical layer. This renders adiabatic boundary layers inviscidly unstable. For the $M = 1.1$ case the least stable mode is a viscous one similar to a Tollmien–Schlichting wave (viscous instabilities are characterised by a growth rate which has its maximum at a finite Reynolds number). At $M = 5.0$ an additional unstable second mode is present. This two-dimensional higher mode shows the largest growth rate and all instabilities are of inviscid nature. Fig. 16 shows the complex frequency $\omega = \omega_r + i\omega_i$ in dependence on the streamwise wavenumber α for the first and second-mode instability (see also Appendix A). Cooling of the wall damps the first but amplifies the higher inviscid modes (Mack, 1987). For strong cooling ($M = 5$, $T_w = T_\infty$, case C) no unstable first mode exists anymore because of the absence of a generalised inflexion point. Instead, the second-mode is unstable over a wide wavenumber range, respectively, it merges with other higher modes (Fig. 16). Also neutral modes exist which will be discussed in the next section.

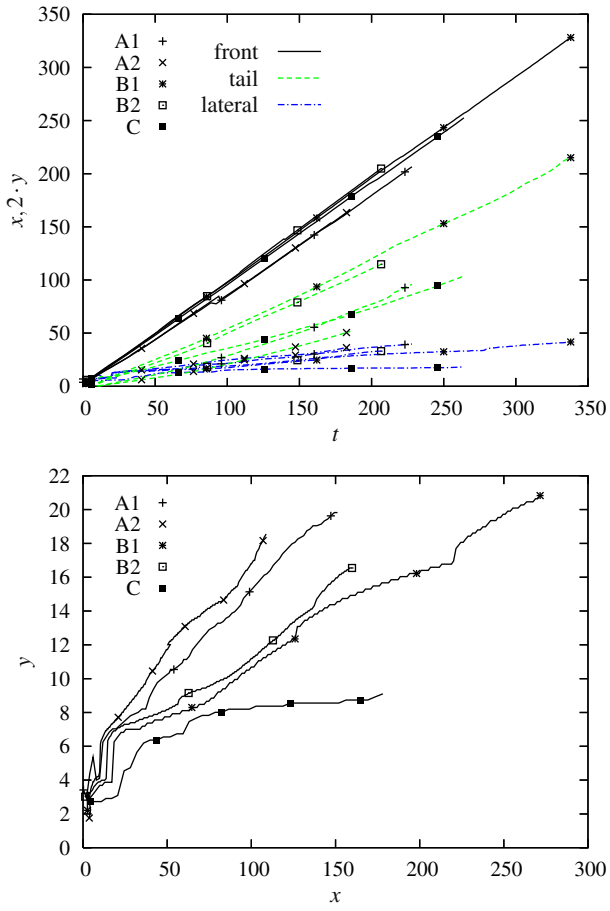

Fig. 15. Location of front, tail and lateral spot edges $|\omega_z| = 0.1$ as function of time (top) and lateral extent as function of streamwise position (bottom).

Table 3
Spot spreading half-angles $\arctan(\Delta y_{la}/\Delta x_c)$

A1	A2	B1	B2	C
5.5°	9.0°	3.0°	5.6°	1.7°

The growth of localised disturbances for the linear instability modes in the limit $t \to \infty$ can be determined with the saddle-point method (see van Saarlos (2003)). We focus on the two-dimensional case specified by the dispersion relation $\omega(\alpha)$. The linear unstable system responds to an pulse initial disturbance with a growing wave packet. Constant growth rates of $\mathrm{Im}(\alpha x - \omega t)$ are found on rays of constant group velocity $\partial\omega/\partial\alpha = x/t$ ($\mathrm{Im}(\partial\omega/\partial\alpha) = 0, \partial^2\omega/\partial\alpha^2 \neq 0$) present in the asymptotic limit. Thus, the wavenumber in the packet changes depending on the location (associated with a specific velocity). While the packet presents the location of rays with positive growth rates, decaying waves neighbouring the packet are present which propagate faster and slower than the packet, respectively. The velocity of the waves is limited by the so-called caustic $\partial^2\omega/\partial\alpha^2 = 0$. Since in our case multiple unstable eigenmodes are present also several wave packets originate from the initial disturbance. Different packets may dominate on different rays x/t. We focus on the evaluation of the velocity of rays with zero growth which describe the edges of wave packets.

For a real long-time development the Reynolds number tends to infinity. For the compressible boundary layers under consideration the presence of instabilities in the inviscid limit makes our problem well suited for the consideration of disturbances in the limit $t \to \infty$. This holds especially for the $M = 5$ cases where the inviscid limit is a reasonable approximation of the stability properties in the Reynolds number range investigated.

For the adiabatic boundary layer at $M = 5$ (cases B1 and B2) the unstable modes *1* and *2* are considered. The propagation velocities of the wave packet boundaries are listed in Table 4. Considering the leading edge, the second-mode instability moves slightly faster than the first-mode instability. In principle, the region of disturbance propagation is surrounded by caustics for every mode.

For the cooled wall the velocity of the corresponding wave packet's leading edge is slightly slower than for the wave packets of the adiabatic wall (Table 4). At the trailing edge the wave packet has special properties. In the range investigated ($\alpha \leqslant 20$), with increasing wavenumber the amplification rate ω_i of the instability mode decays toward zero monotonically (Fig. 16) similarly as shown for the parameters $T_w/T_r = 0.25$, $M = 5.8$ by Mack (1987). Simultaneously ω_r becomes linearly growing in dependence on α. Thus, the trailing edge of the wave packet consists of infinitely high-wavenumbers $\alpha \to \infty$. Its group velocity $\lim_{\alpha\to\infty}\partial\omega/\partial\alpha$ is relatively low compared to the trailing edge velocity of the wavepackets for the adiabatic case (Table 4).

The connection between the non-linear spreading of turbulent spots and the spreading of disturbances according to linear theory has been considered in the literature in the context of front propagation (van Saarlos, 2003). Fronts of chaotic motion spreading into undisturbed areas are classified in the limit of $t \to \infty$ as follows. If the chaotic (turbulent) region spreads faster than the fastest ray of small disturbances with zero growth rate the front is said to be pushed. If the velocity equals the velocity corresponding to zero growth rate, it is called pulled. The underlying assumption is that growing disturbances become non-linear and turbulent because of their large amplitudes. The comparison of two-dimensional linear spreading considered here with the turbulent spot growth is justified in the limit of large developed turbulent spots with a radius of the spot border curvature which is large compared to the wavelength of the considered linear instabilities.

In the following, we assume that the temporal development of cases B2 and C has proceeded long enough to be well approximated asymptotically. The leading edge of the spots (Fig. 15), as well as the hairpins at the tips, propagate approximately with freestream velocity, i.e. faster than linear instabilities spread and, hence, the fronts are pushed. Certainly, in the spanwise direction the fronts are also pushed since there are no linear instabilities. We do not exclude the possibility that the oblique spreading at the wingtips is in some way associated with the spreading of linear instabilities. Also the necessary assumptions for the comparison between wave packets and turbulent spot are only roughly satisfied. Thus, the existence of linear waves on the wingtips (Wygnanski et al., 1979) is not excluded.

For the cooled case, the large velocity difference of the wave packet edges seems to be connected with the fast development of long streamwise structures of the turbulent spot. The slow tail is slightly faster than the trailing edge velocity of the two-dimensional wave packet, while for the adiabatic case it is significantly slower than the trailing edge of any wave packets. If we consider the tail velocity of the iso-contours of λ_2 (Fig. 14), for the cooled case it comes close to the trailing edge velocity of the two-dimensional wave packet: the front is pulled. For the adiabatic case, it is pushed. The spanwise structures at the tail of the spot might also be associated with linear theory according to which slowly propagating two-dimensional disturbances exist. The continuously changing streamwise wavelength of the spanwise structures connected with different velocities in dependence on the wavelength seems to be a phenomenon similar to the changing wavelength within a wave packet according to linear theory. Low-wavenumber

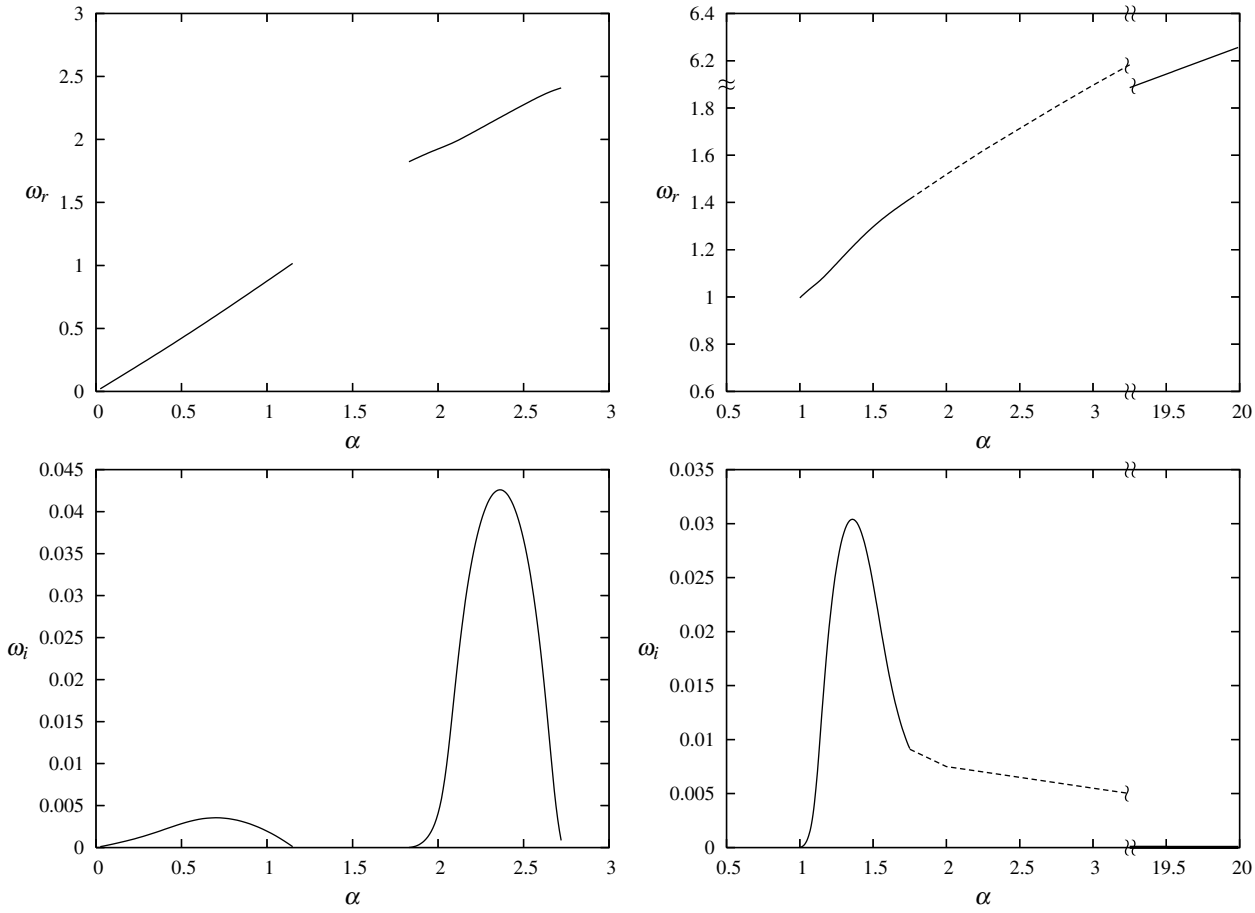

Fig. 16. Dispersion relation $\omega(\alpha)$, unstable modes for $M = 5$, inviscid flow, adiabatic wall (left) and cooled wall (right).

Table 4
Borders of growing wave packets: leading edge velocity u_{le} and trailing edge velocity u_{te}, $M = 5$, inviscid asymptotic analysis

	u_{le}	u_{te}
Adiabatic wall, mode 1	0.95	0.83
Adiabatic wall, mode 2	0.96	0.54
Cooled wall	0.89	0.23

structures propagate further downstream, while high-wavenumber structures follow at the slow tail (Fig. 14).

7. Near-field of turbulent spots

We now focus on the near-field of the turbulent spots. Fig. 17 shows the pressure distribution in the symmetry plane and at the wall for case A2. The core region of the turbulent spot shows relatively high pressure oscillations. The calmed region of the spot is associated with low pressure, whereas further downstream a region of high and another of low pressure follow. The turbulent spot is surrounded by small pressure fluctuations. For case B2 the pressure distribution is visualised in Fig. 18, demonstrating again high fluctuations in the spot core region. Also small pressure disturbances are present in the near-field of the turbulent spot and the calmed region is associated with low pressure. This region is bounded by an expansion wave from near the wall close to the inflow boundary which continues toward the upper computational boundary at approximately the Mach angle. Waves emanating from the trailing edge of turbulent spots were also observed on a cone (see Fig. 1 in Schneider (2004)). The corresponding low Reynolds number cases A1 and B1 have a qualitatively very similar pressure distribution (not shown).

We try to distinguish between two categories of disturbances in the near-field according to their origin. The first one is created directly by the initial disturbance which does not only lead to the localised laminar-turbulent breakdown into a turbulent spot but also persists as small fluctuations in its near-field. The second one is created by the turbulent fluctuations which are present beginning at some later stage of spot formation and are thus created indirectly by the initial disturbance. The turbulent spot, as any turbulence, radiates noise into its near-field. The disturbances farthest away from the spot are determined directly by the initial disturbance. Disturbances close to the spot are affected by the radiation from the turbulent region. These categories are considered separately each for the freestream and the boundary layer region.

For the freestream, the near-field can be described as follows. For the transonic boundary layer (case A2), dominant spherical waves generated from the initial disturbance leave the limited computational domain at an early stage (not shown). The weaker spherical disturbances present in the near-field later ($t = 185$, Fig. 17) are supposed to have their origin in the turbulent region. In case B2, all essential disturbances originating directly from the initial condition are still present in the computational domain at the latest stage of the simulation ($t = 207$, Fig. 18). This is due to the smaller ratio between the propagation velocity of acoustic waves and the flow velocity (see also later in this section). Also spherical waves are present in the freestream.

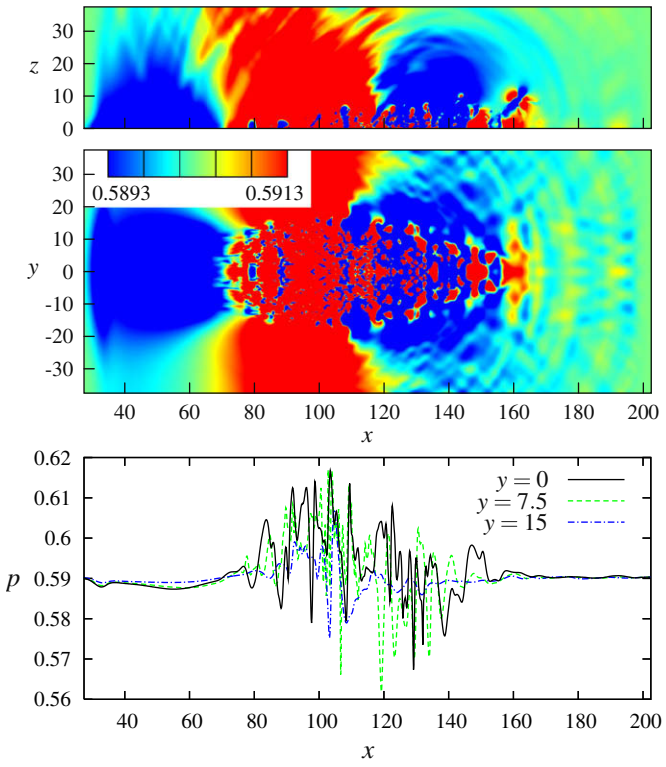

Fig. 17. Pressure p in mid-plane $y = 0$ (top) and at the wall (middle and bottom), $M = 1.1$, $Re = 1500$ (case A2), $t = 185$.

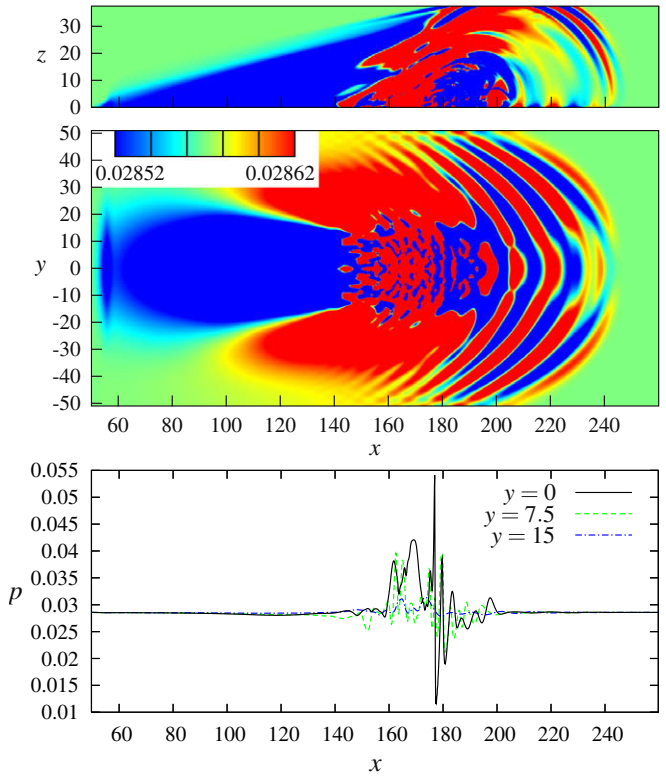

Fig. 18. Pressure p in mid-plane $y = 0$ (top) and at the wall (middle and bottom), $M = 5$, $Re = 5000$ (case B2), $t = 207$.

The nature of disturbances present within the boundary layer differs from that of the freestream. This becomes apparent, e.g., by the fact that the spherical waves in the freestream of case B2 (Fig. 18) do not extend unaltered into the boundary layer. Also the disturbances within the boundary layer are visible as iso-surfaces of λ_2 (Figs. 11 and 13). Their characteristic pattern becomes apparent in the wall pressure distribution shown in Fig. 18 for case B2. The pressure maxima (not minima) in the boundary layer leading the spot are clearly visible as semi-circular structures in the λ_2 visualisation (Fig. 13). (Note that the λ_2 criterion for vortex detection was originally derived for incompressible flow. Iso-surfaces of λ_2 are used here equally for three-dimensional flow structure visualisations at high Mach number. However, the detected structures do not necessarily enclose pressure minima.)

A very similar semi-circular pattern around the front region of the turbulent spot appears at the early stage of development of the transonic cases (shown for A1 in Fig. 3, $t = 59$). It leaves the domain soon after spot triggering before the spot has finally developed (case A1, $t = 228$ and case A2, $t = 185$). At this final stage significant disturbances in the near-field close to the turbulent region are present which are supposed to have their origin in the turbulent region. They are more irregular than the patterns of the early stage (Fig. 3) and those at $M = 5$ (Figs. 12 and 13). Comparing the final stages of cases A1 and A2, the structures in the near-field of the turbulent spot appear to be more dominant for the high Reynolds number simulation (Fig. 11) than for the low Reynolds number one (Fig. 3) at the chosen λ_2 iso-value. Slowly propagating waves originating from the initial disturbance with very low velocity could still be present close to the turbulent region. However, we find no indication that such waves exist or play any role in the transonic boundary layer investigated.

While in the outer region of the pattern of case B2 (Fig. 13) the structures are clearly generated by the initial condition they seem also to be driven by the developed spot despite their very regular appearance. At the wingtips new small oblique structures appear during the whole development. The propagation velocity of the wave pattern in the near-field is higher than the one of the spanwise structures on the bottom of the turbulent region (Section 4). At the same time stage the pattern of case B1 (not shown) has a similar shape and strength as the one of case B2 (Fig. 13). At its final development (Fig. 12) it appears weaker than at earlier stages. Note that the waves originating from periodic neighbours of the spot interact with each other and create interference patterns (see Figs. 11 and 12).

It appears reasonable to consider small disturbances of the near-field within the boundary layer with respect to the linear stability properties of the undisturbed laminar flow. In the freestream, small disturbances propagate according to classical acoustics. Accordingly, besides the unstable modes already discussed, neutral modes are present in compressible boundary layers (inviscid theory).

We now focus on the ordered wave pattern of case B2. The association of the wave phenomenon with a single wavenumber of a linear eigenmode is only possible in an approximate sense since its nature is not two-dimensional and not periodic. We do not consider the spanwise modulation but only the pure streamwise component of the disturbance in the symmetry plane. The regularity of the streamwise oscillations suggests the dominance of a single wavenumber. The semi-circular pattern propagates downstream with a velocity between U_∞ and $U_\infty(1 + 1/M)$. We do not observe any dispersion effects and thus no distinction between group and phase velocity c is made in the following.

Since the streamwise propagation velocity of the wave pattern is higher than the freestream velocity the association with an unstable mode appears impossible since, to our knowledge, there are no such fast instabilities. We are also not aware of slightly damped waves of this spreading velocity. Thus only neutral modes remain as possible candidates. Neutral modes of that velocity are so-called subsonic modes according to their velocity with respect

to the freestream. It is known that if they are present they appear for infinitely many discrete values of the wavenumber α at fixed c (Mack, 1984). In our case a single wavenumber is dominant. The patterns in the near-field of the transonic and the cooled wall boundary layer spots (cases A1, A2 and C) also propagate with a high velocity. One might assume that the phenomenon is also associated with a neutral mode. It is especially apparent for case C that the pattern in the near-field possesses a streamwise changing wavelength. (The boundary layer thickness changes more slowly than this wavelength.)

Another phenomenon of the near-field is the vortex system at the tail of the turbulent spots. In the λ_2 visualisations of cases A1 (Fig. 3), A2 (Fig. 11), B1 (Fig. 12) and B2 (Fig. 13) structures of oblique orientation with respect to the flow direction connected with the spot are present. They look somewhat similar to the stationary waves trailing turbulent spots observed in the wind-tunnel experiment by Chambers and Thomas (1983).

8. Conclusions

Spatial simulations of isolated turbulent spots growing in zero pressure gradient supersonic, adiabatic boundary layers on a flat plate were performed at Mach numbers M of 1.1 (cases A1 and A2) and 5 (cases B1 and B2) at two different Reynolds numbers. The turbulent spots show typical properties known from the literature in the incompressible case. These are, e.g., the arrowhead-like shape of the spot with the downstream overhang region and streaks in the tail region. The turbulent core of the spots shows a trend toward the logarithmic mean flow profile of fully turbulent boundary layers. At high Mach numbers, besides structures known from the incompressible case, additional spanwise structures appear in the front region close to the wall similarly as already observed by Krishnan and Sandham (2006a). The investigation of a cooled wall (case C) at $M = 5$ revealed a highly elongated turbulent spot with a multitude of spanwise vortical structures at its tail in addition to streamwise-elongated structures.

For adiabatic boundary layers, the turbulent spots show some reduction of the lateral spreading with increasing Mach number as discussed by Fischer (1972). However, within our investigated parameter range the spot growth is also Reynolds number dependent, a factor which cannot be separated from Mach number effects.

For $M = 5$ linear stability theory predicts inviscidly unstable modes for which the spreading of wave packets in the limit $t \to \infty$ has been considered. The leading edge of streamwise propagating packets is slightly slower than the turbulent spot front. While in the adiabatic case the trailing edge of the wave packets is significantly faster than the tail of the spot, for strong wall cooling the trailing edge velocities of the wave packet and the turbulent spot are approximately equal, and are very low compared to the adiabatic case trailing edge of the turbulent spot. Thus we suppose that the large streamwise elongation of the cooled case spot is associated with the linear stability properties of the boundary layer.

The initial disturbance triggers waves propagating into the near-field. After the laminar-turbulent breakdown the turbulent core of the spot grows while the surrounding small disturbances spread further. It was shown for all investigated Mach and Reynolds numbers that certain small disturbances spread faster than the turbulent spot develops. Thus, the core of the spot radiates small disturbances into the surrounding laminar environment. Within the boundary layer they form characteristic semi-circular wave patterns. These waves are supposed to be an effect of compressibility. For $M = 5$ a so-called subsonic neutral mode according to the inviscid linear stability theory (Mack, 1984) apparently plays a central role in the formation of the near-field pattern. For our compressible flow simulations, we do not see a necessary connection of these waves in the near-field of turbulent spots with waves discussed previously in the literature that are associated with turbulent spots in incompressible boundary layers.

Acknowledgements

We would like to thank G. Bonfigli, S. Müller, D. Obrist and N.D. Sandham for helpful comments. Computations were performed at the Swiss National Supercomputing Centre (CSCS).

Appendix A. Linear stability

The dispersion relation $\omega(\alpha)$ of linear eigensolutions for two-dimensional inviscid parallel flow has been determined by solving the equation system for the complex amplitude functions $\hat{p}(z)$ and $\alpha\hat{w}(z)$ of the pressure and wall-normal velocity, respectively (Mack, 1987),

$$\hat{w}_z - \frac{U_z\hat{w}}{U-c} = \frac{\mathrm{i}\hat{p}}{\gamma M^2}\frac{\left[T - M^2(U-c)^2\right]}{U-c} \tag{A.1a}$$

$$\frac{\hat{p}_z}{\gamma M^2} = -\frac{\mathrm{i}\alpha^2}{T}(U-c)\hat{w} \tag{A.1b}$$

with the boundary conditions $\hat{w}(0) = \lim_{z\to\infty}\hat{w}(z) = 0$, $\hat{p}_z(0) = \lim_{z\to\infty}\hat{p}_z(z) = 0$, $()_z$ denoting the derivative with respect to z.

References

Adams, N.A., Kleiser, L., 1996. Subharmonic transition to turbulence in a flat-plate boundary layer at Mach number 4.5. J. Fluid Mech. 317, 301–335.
Breuer, K.S., Landahl, M.T., 1990. The evolution of a localized disturbance in a laminar boundary layer. Part 2. Strong disturbances. J. Fluid Mech. 220, 595–621.
Carlson, D.R., Widnall, S.E., Peeters, M.F., 1982. A flow-visualization study of transition in plane Poiseuille flow. J. Fluid Mech. 121, 487–505.
Chambers, F.W., Thomas, A.S.W., 1983. Turbulent spots, wave packets, and growth. Phys. Fluids 26 (5), 1160–1162.
Clark, J.P., Jones, T.V., LaGraff, J.E., 1994. On the propagation of naturally-occurring turbulent spots. J. Eng. Math. 28, 1–19.
de Lange, H.C., Hogendoorn, C.J., van Steenhoven, A.A., 1998. The similarity of turbulent spots in subsonic boundary layers. Int. Commun. Heat Mass Transfer 25 (3), 331–337.
Fasel, H., Thumm, A., Bestek, H., 1993. Direct numerical simulation of transition in supersonic boundary layers: oblique breakdown. In: Kral, L.D., Zang, T.A. (Eds.), Transition and Turbulent Compressible Flows, vol. 151. ASME FED, New York, pp. 7–92.
Fischer, M.C., 1972. Spreading of a turbulent disturbance. AIAA J. 10 (7), 957–959.
Gaster, M., 1968. The development of three-dimensional wave-packets in a boundary layer. J. Fluid Mech. 32, 173–184.
Glezer, A., Katz, Y., Wygnanski, I., 1989. On the breakdown of the wave packet trailing a turbulent spot in a laminar boundary layer. J. Fluid Mech. 198, 1–26.
Henningson, D., Spalart, P., Kim, J., 1987. Numerical simulations of turbulent spots in plane Poiseuille and boundary-layer flow. Phys. Fluids 30 (10), 2914–2917.
Henningson, D.S., 1989. Wave growth and spreading of a turbulent spot in plane Poiseuille flow. Phys. Fluids A: Fluid 1 (11), 1876–1882.
Honein, A.E., Moin, P., 2004. Higher entropy conservation and numerical stability of compressible turbulence simulations. J. Comput. Phys. 201, 531–545.
Krishnan, L., Sandham, N.D., 2006a. Effect of Mach number on the structure of turbulent spots. J. Fluid Mech. 566, 225–234.
Krishnan, L., Sandham, N.D., 2006b. On the merging of turbulent spots in a supersonic boundary-layer flow. Int. J. Heat Fluid 27, 542–550.
Krishnan, L., Sandham, N.D., 2007. Strong interaction of a turbulent spot with a shock-induced separation bubble. Phys. Fluids 19, 016102-1–016102-11.
Lele, S.K., 1992. Compact finite difference schemes with spectral-like resolution. J. Comput. Phys. 103, 16–42.
Levin, O., Henningson, D.S., 2007. Turbulent spots in the asymptotic suction boundary layer. J. Fluid Mech. 584, 397–413.
Lundbladh, A., Johansson, A.V., 1991. Direct simulation of turbulent spots in plane Couette flow. J. Fluid Mech. 229, 499–516.
Mack, L.M., 1969. Boundary-layer linear stability theory. Document No. 900-277 Rev. A, Jet Propulsion Laboratory, Pasadena.
Mack, L.M., 1984. Boundary-layer linear stability theory. Technical report AGARD No. 709, AGARD, Neuilly sur Seine, France.

Mack, L.M., 1987. Review of linear compressible stability theory. In: Dwoyer, D.L., Hussaini, M.Y. (Eds.), Stability of Time Dependent and Spatially Varying Flows. Springer, New York, pp. 164–187.
Maeder, T., 2000. Numerical Investigation of Supersonic Turbulent Boundary Layers. Ph.D. thesis, ETH Zurich.
Mee, D.J., 2002. Boundary-layer transition measurements in hypervelocity flows in a shock tunnel. AIAA J. 40 (8), 1542–1548.
Ng, L.L., Erlebacher, G., 1992. Secondary instabilities in compressible boundary layers. Phys. Fluids A: Fluid 4 (4), 710–726.
Pirozzoli, S., Grasso, F., Gatski, T.B., 2004. Direct numerical simulation and analysis of a spatially evolving supersonic turbulent boundary layer at $M = 2.25$. Phys. Fluids 16 (3), 530–545.
Riley, J.J., Gad-el-Hak, M., 1985. The dynamics of turbulent spots. In: Davis, S.H., Lumley, J.L. (Eds.), Frontiers in Fluid Mechanics. Springer, Berlin, pp. 123–155.
Sandham, N.D., Adams, N.A., Kleiser, L., 1995. Direct simulation of breakdown to turbulence following oblique instability waves in a supersonic boundary layer. Appl. Sci. Res. 54, 223–234.
Sandham, N.D., Li, Q., Yee, H.C., 2002. Entropy splitting for high-order numerical simulation of compressible turbulence. J. Comput. Phys. 178, 307–328.
Sankaran, R., Sokolov, M., Antonia, R.A., 1988. Substructures in a turbulent spot. J. Fluid Mech. 197, 389–414.
Schmid, P.J., Henningson, D.S., 2001. Stability and Transition in Shear Flows. Springer, New York.
Schneider, S.P., 2004. Hypersonic laminar-turbulent transition on circular cones and scramjet forebodies. Prog. Aerosp. Sci. 40, 1–50.
Schröder, A., Kompenhans, J., 2004. Investigation of a turbulent spot using multi-plane stereo particle image velocimetry. Exp. Fluids 36, 82–90.
Singer, B.A., 1996. Characteristics of a young turbulent spot. Phys. Fluids 8 (2), 509–521.
Singer, B.A., Joslin, R.D., 1994. Metamorphosis of a hairpin vortex into a young turbulent spot. Phys. Fluids 6 (11), 3724–3736.
Stewartson, K., 1964. The Theory of Laminar Boundary Layers in Compressible Fluids. Claredon Press, Oxford.
Stolz, S., Schlatter, P., Kleiser, L., 2007. Large-eddy simulations of subharmonic transition in a supersonic boundary layer. AIAA J. 45 (5), 1019–1027.
van Saarlos, W., 2003. Front propagation into unstable states. Phys. Rep. 386, 29–222.
Williamson, J.H., 1980. Low-storage Runge–Kutta schemes. J. Comput. Phys. 35, 48–56.
Wygnanski, I., Haritonidis, J.H., Kaplan, R.E., 1979. On a Tollmien–Schlichting wave packet produced by a turbulent spot. J. Fluid Mech. 92, 505–528.